metals

MDPI

Article

Towards Manufacturing of Ultrafine-Laminated Structures in Metallic Tubes by Accumulative Extrusion Bonding

Matthew R. Standley and Marko Knezevic *

Department of Mechanical Engineering, University of New Hampshire, Durham, NH 03824, USA; mrx46@wildcats.unh.edu

* Correspondence: marko.knezevic@unh.edu

Abstract: A severe plastic deformation process, termed accumulative extrusion bonding (AEB), is conceived to steady-state bond metals in the form of multilayered tubes. It is shown that AEB can facilitate bonding of metals in their solid-state, like the process of accumulative roll bonding (ARB). The AEB steps involve iterative extrusion, cutting, expanding, restacking, and annealing. As the process is iterated, the laminated structure layer thicknesses decrease within the tube wall, while the tube wall thickness and outer diameter remain constant. Multilayered bimetallic tubes with approximately 2 mm wall thickness and 25.25 mm outer diameter of copper-aluminum are produced at 52% radial strain per extrusion pass to contain eight layers. Furthermore, tubes of copper-copper are produced at 52% and 68% strain to contain two layers. The amount of bonding at the metal-to-metal interfaces and grain structure are measured using optical microscopy. After detailed examination, only the copper-copper bimetal deformed to 68% strain is found bonded. The yield strength of the copper-copper tube extruded at 68% improves from 83 MPa to 481 MPa; a 480% increase. Surface preparation, as described by the thin film theory, and the amount of deformation imposed per extrusion pass are identified and discussed as key contributors to enact successful metal-to-metal bonding at the interface. Unlike in ARB, bonding in AEB does not occur at ~50% strain revealing the significant role of more complex geometry of tubes relative to sheets in solid-state bonding.

Keywords: plasticity; strength; metallic tubes; finite element analysis; accumulative extrusion bonding

Citation: Standley, M.R.; Knezevic, M. Towards Manufacturing of Ultrafine-Laminated Structures in Metallic Tubes by Accumulative Extrusion Bonding. *Metals* **2021**, *11*, 389. https://doi.org/10.3390/met11030389

Academic Editors: Andrew Kennedy, Gabriel Centeno Báez and Maria Beatriz Silva

Received: 15 January 2021
Accepted: 23 February 2021
Published: 27 February 2021

1. Introduction

Bimetallic materials have been used for components delivering different material properties by their geometry (e.g., inside versus outside of a tube) [1–4]. Such components achieve benefits, such as lower cost for the consumer and producer, reduced weight, simplification of design, and/or reduced number of parts in a structure or assembly [3]. Bimetallic materials could be manufactured in the form of tubular geometries to serve desired applications. When employing bimetallic tubes, for example, one material can provide strength and stability, while the other can offer better corrosion resistance. A two-layer copper-steel tube, for example, can handle high loads via the steel and the corrosion resistance via the copper [4].

Bonding between the bimetals is not always necessary, and ultimately depends on the application. The two-layer designs typically rely on each material to perform one aspect of the intended design function independent of the other. In this case, a very tight compression fit between the two constituent metals may be appropriate. Evolving from the two-layer concept, multilayered material is envisioned for even more demanding or unique applications. To this end, multilayered materials provide a blended, and most often optimized, set of material properties but require each layer to be bonded to the next to do so.

Multilayered bimetallic manufacturing is a relatively new frontier in manufacturing and delivers superior material characteristics when compared to the constituent materials.

Many material combinations have been reported as bonded using accumulative roll bonding (ARB) such as Cu/Ti [5], Al/Cu [6], Al/Zn [7], Mg/Al [8], Cu/Zn/Al [9], Cu/Zn [10], Zr/Nb [11,12], Mg/Nb [13,14] and Zn/Sn [15] in plate form. When the layering is pushed to the ultrafine micron, or ultimately nanometer scale, the multilayered bimetallic material exhibits significantly improved strength [16–24], thermal stability [25,26], resistance to shock damage [27], and resistance to radiation damage [28,29]. Beyond this, the authors of [30] summarize the history of laminated metal composites and other benefits of bimetallic materials, such as improved fracture resistance, delayed fatigue crack growth, and ballistic energy absorption.

This work explores a processing methodology for manufacturing multilayered bimetallic tubing to achieve similar improvements in material properties to ARB sheets. To the knowledge of the authors at the time of publication, no research has reported producing multilayered bimetallic tubing using any severe plastic deformation processes. Following previous research in extrusion to achieve bimetallic tubing [31], this work takes inspiration from their design to develop a more complete manufacturing process. The process is termed accumulative extrusion bonding (AEB) and is used, in an iterative sense, to create single metal and bimetallic tubing with several layers. AEB, like ARB, is a severe plastic deformation process, which is defined as a metal forming process that creates very high strain without significant change to the overall dimensions to produce substantial grain refinement using severe straining and high levels of hydrostatic pressure [11,32–39]. By doing so, a decrease in grain size can improve the material properties following the Hall-Petch relationship [40–42] and increase the material strength by a factor of three to eight [43]. Additionally, as reported in [44], materials with ultrafine grains can have good damping properties, exhibit lower temperature super-plasticity, and high magnetic properties.

The AEB process involves iterative extrusion, cutting, expanding, restacking, and annealing. Due to the increased complexity of maintaining the geometrical shape of tubing relative to sheets, AEB is a much more challenging process than ARB. Other severe plastic deformations processes exist to produce extruded tube, and are well documented in the following review article [45]. Such processes include Equal Channel Angular Pressing (ECAP), Tube Channel Pressing (TCP), Tubular Channel Angular Pressing (TCAP), among others [45–47]. Since restacking and reprocessing is essential in producing ultrafine grains in multilayered tubing, AEB is described herein.

When this AEB process is compared to other AEB processes, the main differences include geometry of the extruded material, the custom dies and setup used, and the expansion process. Additionally, AEB performed in [48] did not use intermittent annealing, and because of this, tracked the true strain increase as samples were continuously processed. The AEB process used in the present research, utilizes annealing after every severe plastic deformation step such that accounting for continuous strain is not needed as strain effects are removed. Additionally, no material specimen or die preheat is used as indicated in the research performed in [49]. Most unique, no research has reported using AEB to manufacture multilayered bimetals in the form of tube as current research utilizes plate or sheet as done in [48–51]. For this reason, as part of the AEB process used for this research, expansion is necessary to facilitate restacking.

Two sets of specialty tooling are designed for a hydraulic press: One imparting 52% radial strain and another imparting 68% radial strain to produce the tubing. The design process is aided by finite element (FE) simulations to better understand the mechanics of the severe plastic deformation operations. After making the tooling, several similar and dissimilar metallic tubes are created to evaluate the extent of bonding, microstructure, and material properties. Hardness of the materials, yield strength, and ultimate tensile strength are compared before and after processing. Moreover, grain structure and the amount of bonding at the metal-to-metal interfaces are measured using optical microscopy. Surface preparation and the amount of deformation imposed per extrusion pass are discussed as critical to successful metal-to-metal bonding at the interface. Future work will attempt to create ultrafine multilayered bimetallic tubes with micron to nano radial lay-

ers of alternating material with many metal-metal interfaces governing a unique set of material properties.

2. Methods

2.1. Theory of Bonding

The thin film theory prevails as the primary explanation for bimetal bonding in high pressure cold rolling. Like rolling, extrusion is also a high-pressure process in which the theory is viable as other mechanisms that explain bonding are unlikely to occur. Other such bonding mechanisms are diffusion, overcoming energy barrier, and joint recrystallization [52]. A brief summary of the theory is as follows:

1. A very thin brittle surface must exist on both metallic faces to be bonded.
2. Under high pressure, the metallic faces are forced into one interface where the thin brittle surfaces on both metals begin to crack under a significant amount of imposed strain.
3. Through the small cracks fresh virgin material extrudes which interact with the opposing virgin material to form a metallic bond.

In ARB applications, the brittle surfaces are prepared by light scratch brushing using stainless brushes, and the high pressure is provided by rolls. For example, nickel plated Cu/Al [53], Mg/Nb [13], Al/Ni [54], and Al/Al [55] sheets were produced using this technique. In this work, high pressure is provided by a die, a mandrel, and a punch mounted in a hydraulic press. The theory and extrusion process are depicted schematically in Figure 1. In stage 1, as indicated by the bubble numbers, the two metal tubes are under compression due to the punch (not shown), and an initial air gap is present at the metal-metal interface. This surface must be as clean as possible, free of any contamination, and prepared such that a thin brittle surface exists. As the material is forced into the extrusion ledge in stage 2, the air gap is significantly reduced, the metal-to-metal interface is formed, and plastic strain occurs within the metals. Due to the high strain levels, cracks form within the thin brittle surfaces, and virgin material of each metal extrudes through the cracks, interact, and bond. Entering stage 3 completes the extrusion process by providing the final desired shape: a reduced outer diameter and maintained inner diameter of a new tube size. Some areas may not bond, and voids may become present. Further processing, by repeating the process shown in Figure 2, will continue to thin and stretch the interfaces such that voids, and trapped oxides will be thinned and blended into the metallic structure where their influence on material behavior is minimized [13].

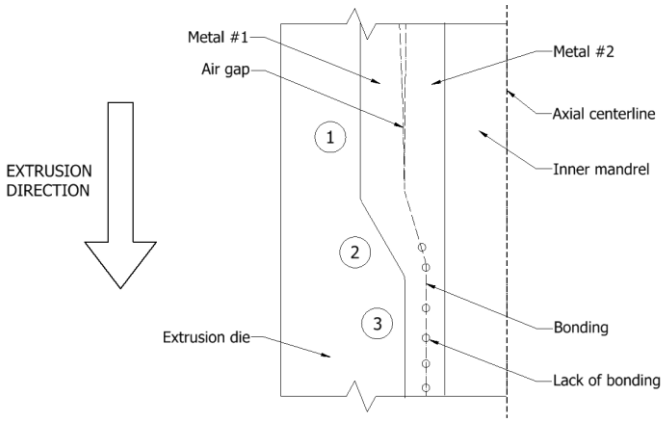

Figure 1. Axis-symmetric cross section of extrusion process and the three stages of bonding using AEB. The metal initially experiences compression (stage 1) before entering the extrusion zone (stage 2), where severe plastic deformation occurs, and exits in the final desired shape (stage 3).

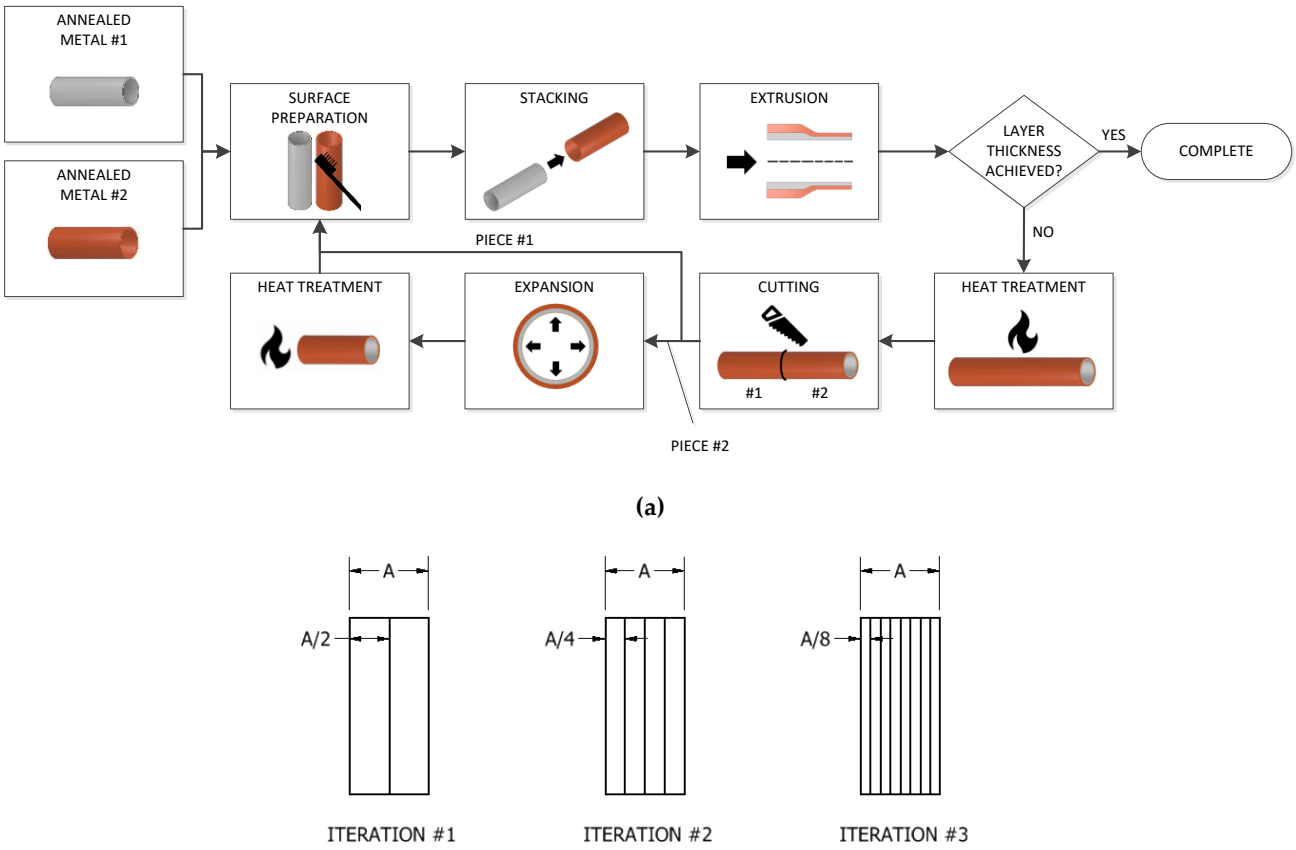

Figure 2. (**a**) The manufacturing process flow map for achieving ultrafine-laminated structures in metallic tubes via AEB. (**b**) Graphical visual of the nominal layer thickness within the tube wall when a bimetal is processed multiple times using AEB. When processing using AEB, the wall thickness is maintained while individual layers exponentially decrease. Note that processing steps, such as cleaning and expansion, will impact layer thicknesses and overall wall thickness such that each individual layer is not expected to be exactly the same.

2.2. Manufacturing

To achieve multilayered bimetallic tubing, it is essential to introduce an iterative process to obtain layers expediently. As the process is iterated, the layer thicknesses within the tubular wall exponentially decreases, while the number of layers exponentially increases using the process flow detailed in Figure 2. Unlike the research in [56], which manufactured bimetallic tube from solid billets of copper and aluminum, the starting base material is tube since tubes are ubiquitous and can be purchased such that they initially stack together.

The first process step is surface preparation of initially annealed tubes followed by stacking. Surface preparation is important to remove foreign material and naturally occurring oxides which can hinder bonding. Additionally, during this step, the surfaces to be bonded must be hardened as described by the thin film theory. Once prepared, one metal tube is inserted into the other metal tube and then the stacked tube is extruded by decreasing the outer diameter and maintaining the inner.

If the desired laminated layer thickness is not achieved, then the metals are prepared for another iteration as shown in Figure 2. The first step to prepare the extruded tube for reprocessing is annealing to restore ductility and bisection at the midpoint to create two tubes of approximately half the extruded length. One of the two metal tubes is then expanded such that it can fit over its extruded diameter. After another annealing of the expanded tube, the initial process is repeated. This continues until the desired layer

thickness is achieved. The exponential decrease in layer thickness, occurring at 2^i, is critical in achieving very thin layer thicknesses in a reasonable way.

The two annealing steps, and the initial annealing, are critical to processing and are tactically used to restore ductility before all severe plastic deformation process steps. Based on testing performed, herein, the process flow shown in Figure 2 is the minimum process flow required. Bimetallic tubes produced when omitting any of the annealing steps, for example, caused blistering and tearing during extrusion or expansion.

2.2.1. Surface Preparation

The stacking operation is the simple action of inserting one metal tube into the other. Before this operation is performed, it is critically important to prepare the surfaces, which will become the metal-to-metal interface. In ARB, the interfacial surfaces are typically degreased using acetone and then scratch-brushed with stainless steel bristles [13,53–55]. This surface preparation is reportedly one of the most important steps to achieve full bonding, since it removes the naturally occurring oxide layer and hardens the surface simultaneously. The scratch brushing creates a slightly hardened and brittle outer surface in comparison to the bulk material, due to local strain hardening occurring at the surface. The brittle surface, which will be prone to cracking during extrusion, will allow virgin sub-surface metal to pass through the cracks to contact the virgin material of the other metal to enact bonding. Scratch brushing is applied transverse to the extrusion direction to help promote crack opening.

Before stacking and scratch brushing, acid cleaning is performed to remove any surface impurities. The copper was cleaned by pickling using a solution of 10% sulfuric acid and 90% distilled water per volume. This was done at room temperature for 10 min. After, the acid was neutralized with cool distilled water. The copper was then degreased in an ultrasonic acetone bath for 30 min, where the acetone was drained and replenished halfway through the cleaning process. The aluminum only received degreasing using the ultrasonic acetone bath. After degreasing in acetone, the metal tubes were scratch-brushed and stacked together.

To achieve the most optimal hardened surface, tubes were scratched with stainless steel bristles. The outer diametrical interface was scratched with a handheld stainless-steel brush, while the inner diametrical interface was brushed with a rotary stainless-steel brush. The stainless-steel bristles were 25.4 mm long on the handheld brush with a diameter of 0.305 mm. The stainless-steel bristles on the rotary brush were 13.97 mm long with a diameter of 0.152 mm and rotated at a constant RPM during application. The two different methods of applications were employed due to the curved geometry of each surface.

The surface roughness was measured before and after brushing and is tabulated in Table 1. Surface roughness increased 29.6% and 46.8% respectively on the inner, and outer surfaces, respectively. To find the average surface finish, measurements were taken in 10 random locations on each surface using a Pocket Surf III profilometer (Mahr Federal Inc., Providence, RI, USA). All surface finish values reported before and after brushing are representative of cold extruded aluminum using lubricant for context [57].

Table 1. Average surface roughness before and after scratch brushing.

Process	Surface	Material	Before μm RA$\surd$	After μm RA$\surd$	% Increase
Rotary brush	Inner diameter	Copper	1.15	1.49	29.6
Handheld brush	Outer diameter	Aluminum	0.32	0.47	46.8

The intent of the brushing is not to induce visible asperities and significantly increase the surface roughness, but to clean the surface of oxidation while hardening it at the same time. Oxidation layer minimization is necessary to aid in bonding, but significantly over-brushing did not improve the amount of bonding. Not quantified by the authors, but reported in literature [52], minimizing the build-up of oxidation is critical to aid in bonding

and to reduce additional foreign material inclusion. Beyond scratch brushing, minimizing contact with the atmosphere was employed to discourage further oxidation growth.

After scratch brushing the metal tubes are not cleaned of any debris caused by brushing. Instead, the tubes were lightly tapped to remove any loose particles. Immediately following the acetone cleaning and brushing, the tubes were stacked and extruded. On average, this was performed within 2 min to prevent the naturally occurring oxide layer to fully reform. After 15 min of exposure to air, as reported in another study [58] regarding aluminum bonding, the natural oxide layers begin to markedly interfere with the bonding process.

The scratch brushing method does not produce any noticeable debris from the stainless steel bristles which helped promote cleanliness. Other methods beyond scratch brushing were attempted but were ultimately not used. Metal files, Scotch-Brite™ pads (3M Company, Saint Paul, MA, USA), and various sanding papers were also used with no success. The major issue with these methods is cleanliness control and the lack of versatility to be applied to curved surfaces of the inner and outer diameters. These methods created a lot of non-metallic debris during application and caused too much inconvenience during processing.

2.2.2. Extrusion

The extrusion process bonds the two metals together through severe plastic deformation as described by the thin film theory. Previous research in die geometry has determined an outer ring die paired with a straight mandrel produces the least peak stresses within the die and can successfully achieve enough plastic strain to promote bonding [31]. Therefore, the die angle and geometry are adopted for this research. Figures of the die are presented in the next section. The extrusion process is performed in a 4-pronged die set which was customized to support a self-aligning die and punch. The die, punch, and mandrel are used to maintain the tubular shape and are described in more detail in the die design section. The extrusion was performed at room temperature (approximately 20.5 °C) with an extrusion speed of 2.73 mm/s. No heat was added during extrusion to promote bonding.

The die, mandrel, and punch are coated with a thin layer of extrusion oil to reduce friction and discourage material adhesion. Non-diluted Drawsol® WM 4740 (Houghton International, Manchester, England) was used for its ability to maintain high film strength when under extreme pressure. This oil is also recommended for various metals including steel, stainless-steel, titanium, and aluminized alloys. From a processing perspective, this synthetic lubricant is water soluble, which is easily removed with running tap water.

Bimetals are extruded at 52% and 68% deformation which represent how much the outer diameter is reduced during extrusion. These values represent the minimum (50%) [5–9] and mid-range of reported deformation employed in previous research, which achieved bonding using ARB. These deformation values also promote stacking as well; at 52% deformation a 2-layer tube can be re-stacked, and the original die can be reused, while at 68% deformation, 3-layer tube stacking can be utilized. This was done intentionally to reduce the number of required dies. In both cases, the deformation percentage values are slightly more than 1/2 and 2/3 as to provide clearances from the nominal stacking fraction to assist in processing.

2.2.3. Cutting

The second step in the iterative loop, if the bimetallic layer thickness is not achieved, is cutting. Simply, the bimetal is cut to remove the non-bonded section at the end of the bimetallic extrusion, the non-bonded initial section at the start, and then equally in half perpendicular to the extrusion direction. By performing cutting the total material volume is not conserved. Therefore, it is necessary to quantify the expected losses per iteration to ensure a viable end-product is produced. Cutting is performed using a material specimen preparation sawmill using a diamond infused metallurgical cutting disc. After, all edges were deburred with 320 grit sandpaper.

2.2.4. Expansion

One of the two extruded tubes require diametrical expansion to facilitate stacking. The chosen tube is expanded such that the inner diameter is increased to a size that is slightly larger than the outer diameter of the extruded tube. This is performed by pushing the tube over a diametrical expansion mandrel. The expansion mandrel utilizes a cylindrical section that tapers at 10° to an enlarged diameter. The punch, which pushed the bimetal into the extrusion die, is the same punch used to push the tube over the expansion ledge. The bimetal is passed over the expansion post multiple times to fully remove spring-back and achieve a cylindrical tube for stacking. The expansion mandrel is described in more detail in the die design section. Other options to expand the tube were considered such as metal spinning as described in [59,60]. Ultimately, it is more desirable to expand the tube using a mandrel because the process is simple, easy to control, and contained to the same experimental setup (i.e., the hydraulic press and die set).

The expansion step does not promote or impact bonding at the interface since bonding occurred during extrusion where significantly large strains (compared to strains experienced during expansion) are imposed. Additionally, from a conservation of volume perspective, the wall thickness of the expanded tube will decrease depending on the amount of deformation imposed (~11% and ~8% for the 52%, and 68% deformation cases, respectively), which will impact layer thickness consistency. Even though wall thicknesses become slightly inconsistent as iterations continue, the intent is to create many interfacing layers, i.e., the ultrafine structures independent on local layer thicknesses. The local deformation conditions also cause non-uniformity in layer thickness.

2.2.5. Heat treatment

During the extrusion and expansion processes, the metal experiences severe plastic deformation, which is causing significant strain hardening. To aid in processing, it is necessary to restore ductility. Additionally, research in ARB, which is similar to AEB, requires intermediate annealing [61]. Initial annealing of the as-received material is performed to remove initial tempers of T6 for aluminum and H58 for copper. The as-received copper is annealed to 426 °C with a 1 h soak time and cooled at a rate of 426 °C/h. The as-received aluminum is annealed to 413 °C with a 2.5 h soak time and cooled at a rate of 28 °C/h. The initial annealing was selected to enhance ductility [62].

Intermediate annealing is performed after every iteration, and the same annealing as described above for annealing aluminum was employed on the bimetal copper-aluminum tubes produced. It was found that annealing was necessary in every iteration step. Multilayered bimetals were attempted with the annealing step omitted, and severe blistering and tearing occurred throughout the tubular wall.

3. Die and Expansion Designs

The experimental setup of the extrusion process is shown in Figure 3a. The setup is installed in a hydraulic press capable of 260 kN (Greenerd Press and Machine Co., Nashua, NH, USA). The press is omitted from figures. As indicated previously, extrusion was performed at 52% and 68% radial strain. The only difference between the two extrusions is the size of the extrusion ledge (i.e. the dimension L, as shown later) to increase the strain from 52% to 68%. The off-the-shelf die set is customized to perform both the extrusion and expansion processes. The extrusion die and the expanding post are easily swapped to either perform the extrusion or expansion process. A cut-away view of the extrusion setup is provided in Figure 3b,c. Critical dimensions are shown in Figure 3c and are tabulated in Table 2.

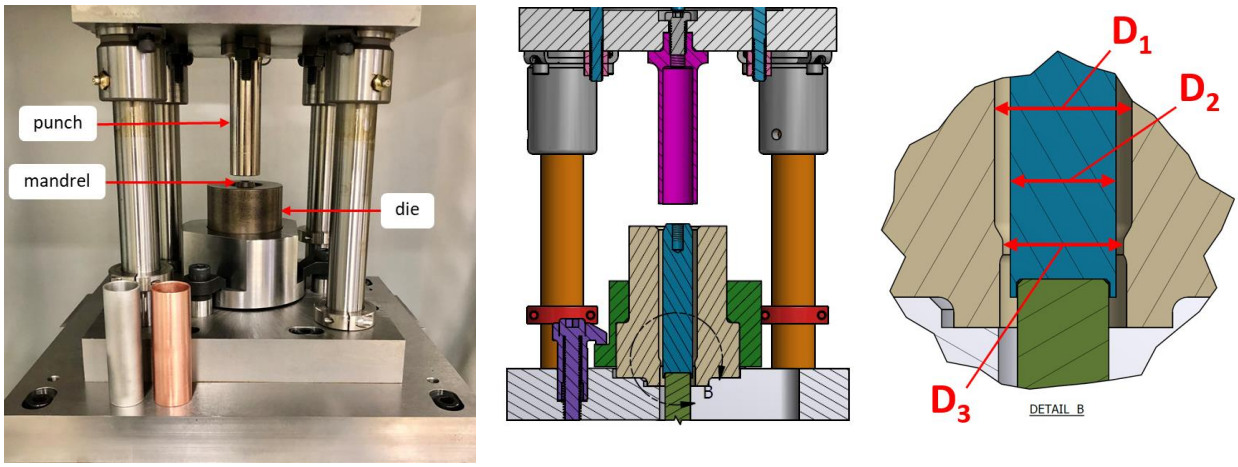

(a) **(b)** **(c)**

Figure 3. (**a**) Experimental setup of extrusion process which provides 52% radial strain. Omitted is the hydraulic press. Also depicted is annealed copper and aluminum test metals ready for extrusion. For size perspective, the test metals are 89 mm in height. This setup is identical to the process which enacts 68% radial strain except for dimension L. (**b**) Section view of extrusion setup. (**c**) Die cavity and extrusion ledge. The tubular bimetal is omitted.

Table 2. Critical dimensional values of extrusion die.

Deformation	D_1 mm	D_2 mm	D_3 mm
52%	28.70	22.07	25.25
68%	28.70	22.07	24.18

For either the extrusion or the expansion process, both configurations utilize the punch as the mechanism to enact deformation. This was tactically chosen to keep the setup contained to one die set installed in one hydraulic press. Both the die and the expansion post use a floating alignment method. To ensure the punch is always axially aligned neither the extrusion die, nor the expansion post are fixed in place; rather, they both self-align to the punch during setup.

The die is of sufficient length to fully encapsulate the length of the bimetal tubes. This is to ensure it is forced into the extrusion ledge. The extrusion edge geometry, which has a 30° transfer from the initial diameter to the extrusion diameter, has rounded and smooth radii. Just below the extrusion ledge is a diametrical relief for ease of tube removal after the tube is extruded into and past the extrusion ledge. The inner mandrel floats collinear to the die and remains collinear when the bimetal tubes are installed inside the die. The floating mandrel is positioned such that only the least amount of the mandrel is below the extrusion ledge to aid in the removal of the bonded bimetal tube. After extrusion is performed, due to the setup in a hydraulic press, the bimetal tube is removed by removing the die and floating mandrel. For this reason, the floating mandrel is not attached to the vertical support below it. A relief is cut into the bottom portion of the die set, the width slightly larger than an extruded tube, to assist in bimetallic tube removal. Lastly, the punch is designed to insert into the die and have the floating mandrel insert in it. Clearances between these components are less than 2.54×10^{-2} mm.

The expansion post for the expansion process, shown in Figure 4, has a smooth transitional ledge, at 10°, used to expand the bimetal tube such that it can fit over a tube of its original extruded size. A few variations of the expanding post can be used in which the expansion diameter is increased in predetermined increments to aid in processing. Incorporating these variations allows a step-up approach to achieving the final desired inner diameter of an expanded bimetal, if needed. Alternatively, the diameter may be increased directly in one expansion step. For the testing performed, all tubes were directly

expanded in one step. Sitting at the base of the expanding post is an oversized washer which can be used to aid in the removal of the bimetal.

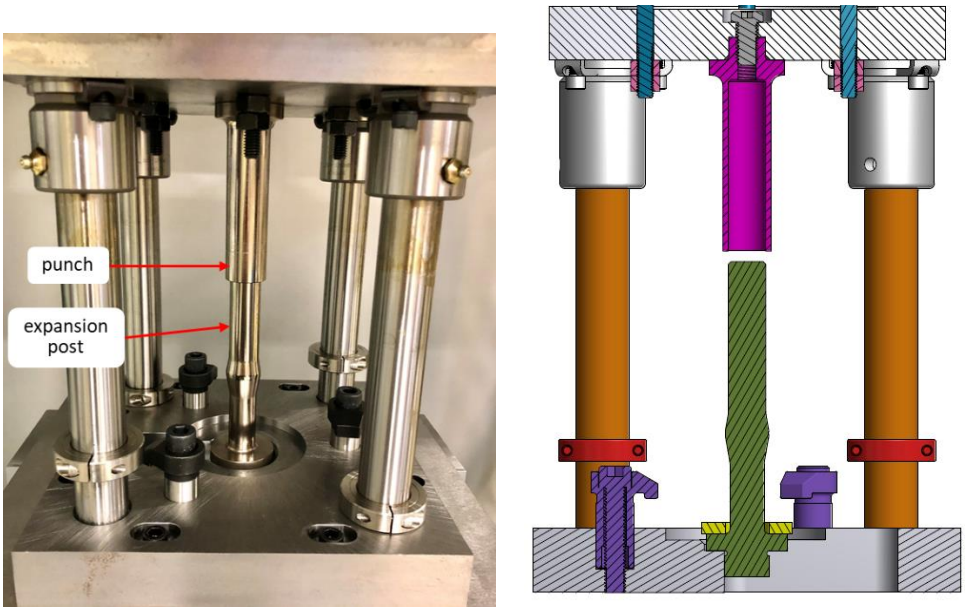

(a) **(b)**

Figure 4. (**a**) Experimental setup of expansion process. Omitted is the hydraulic press. (**b**) Section view of expansion setup. Expansion setup uses the same die set as the extrusion process.

The die, punch, mandrel, and expansion post are the main functional components that are performing the extrusion or expansion. The material for these components is AISI A2 tool steel. This material is commonly used in extrusion dies and other high stress material forming processes. The hardness range for these components is 58 to 62 HRC which is a typical range for extrusion and forming dies. The A2 material has desirable characteristics which are tabulated in Table 3. The wear resistance and toughness are improved with the coating described below.

Table 3. Cold work tool steel relative ratings (A = greatest to E = least) [63].

Characteristic	AISI A2 Tool Steel
Safety in hardening	A
Depth of hardening	A
Resistance to decarburization	B
Stability of shape in heat treatment	A
Machinability	E
Hot hardness	C
Wear resistance	B/C
Toughness	E

The die, punch, mandrel, and expanding post are coated in a thermal diffusion process, which is a typical coating process for blanks, dies, and components used in similar high stress forming operations. The coating provides additional lubricity and reduces reactionary stresses during extrusion. Additionally, the tool toughness and hardness are promoted, and in general, the life of the components are extended. The coating data is tabulated in Table 4.

Table 4. Coating data for die, mandrel, punch, and expansion post [64].

Coating Information	Result
Thickness (μm)	5.08–7.62
Micro hardness (HV)	3500–3800
Coefficient of friction	0.08
Composition	Vanadium carbide

4. Materials

The initial aluminum tube (Ø25.40 mm × 1.65 mm) is 6061 per ASTM B210 and the initial copper tube (Ø28.58 × 1.65 mm and Ø25.40 mm × 1.65 mm) is C12200 per ASTM B75. The true stress-strain curves of the materials, after initial annealing, are presented in Figure 5. Flow curves were determined per ASTM E8 using the bulk tube as the specimen.

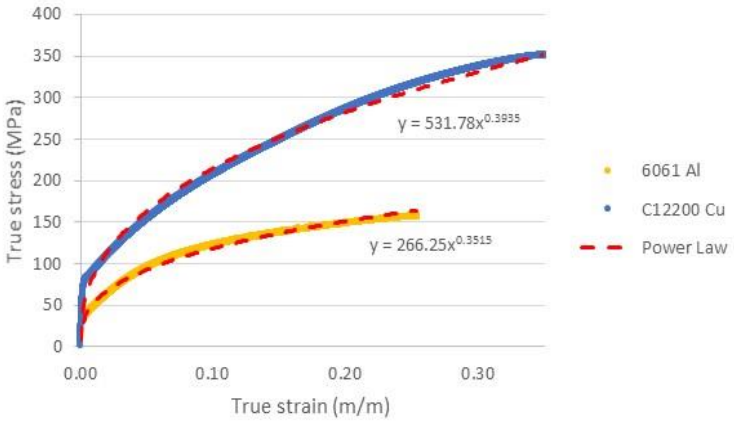

Figure 5. True stress-strain curves of annealed copper and aluminum. Material behavior is modeled by the power law.

Before processing, the as-received material is annealed since the aluminum and copper were tempered to T6, and H58, respectively. Both initial annealing cycles were performed as recommended by the Society of Manufacturing Engineers to produce optimally ductile materials as previously described. To confirm the effectiveness of the initial annealing, hardness measurements were taken; the results are shown in Table 5. The copper experienced a 60.2% decrease in hardness and the aluminum experienced a 67.8% decrease. Knoop hardness testing was performed using a 500 g force held for 10 to 15 s where the hardness value was averaged over 10 samples.

Table 5. Hardness of mill and annealed material (HK).

Material	Mill	Annealed
Copper	141.1	56.1
Aluminum	126.4	40.7

The copper and aluminum material behavior are fitted with the power law with an R^2 value of 0.9816, and 0.9893, respectively. Figure 5 shows that the copper and aluminum exhibit strain-hardening which is represented well by the power hardening law shown in Equation (1):

$$\sigma = K\varepsilon^n \quad (1)$$

The strength coefficient, K, and the strain hardening exponent, n, are presented in Table 6. An important item of note is the dissimilarity between both materials true stress-strain curves. For consistent plasticity to occur within both metals, and to maintain balanced layer formation, similar flow stress behavior across the material is tactically sought; however,

the copper has a strength coefficient 99.7% larger than the aluminum, which is expected to influence the difference between extruded layer thicknesses. The values of the strain hardening exponent represent how quickly the material hardens when deforming. A value closer to zero represents a material resisting deformation, while the values closer to one represent a material where true stress and true strain vary proportionality.

Table 6. Power law strength coefficient and exponent.

Material	Strength Coefficient *K*, MPa	Strain Hardening Exponent *n*
Copper	531.78	0.3935
Aluminum	266.25	0.3515

5. Finite Element Method-Based Simulations of Extrusion

The extrusion process is modeled in ANSYS Mechanical (ANSYS 19.1., ANSYS Software Company, Canonsburg, PA, USA) to gain insight on the plastic behavior of the bimetal and to understand the stresses that develop within the die. The geometry of the extrusion model consists of four components: Two metals experiencing extrusion and two workpieces enabling the extrusion. The two metals are referred to as the outer and inner metals, which represent the initial outer, and inner diametrical layers, respectively. For all simulations and experiments, the copper is always the outermost metal tube. The model is axisymmetric and 2-dimensional. Figure 6a shows the ANSYS model of the extrusion process, where axis symmetry is taken about the farthest left edge. The geometry represents a 2-dimensional "slice" of the area-of-interest, which is the lower section of the die and mandrel identified by the red circle in Figure 6b. The model is axisymmetric and 2-dimensional because no 3-dimensional irregularities in stress or strain are expected since the tooling is precision-ground and the design utilizes a self-centering die.

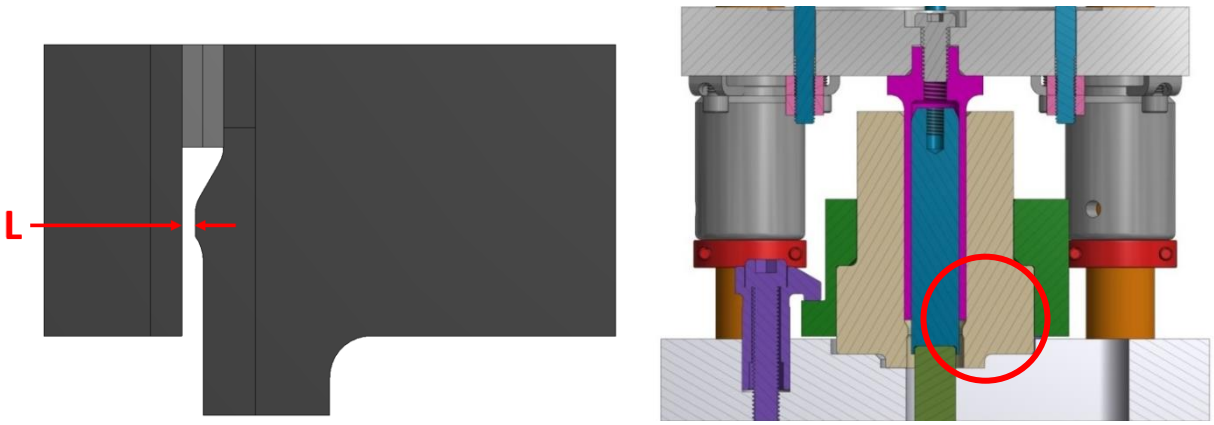

(**a**) (**b**)

Figure 6. (**a**) Finite element geometry which represents the two deformation cases studied: 52% and 68%. Dimension L was adjusted to obtain the two different cases. (**b**) The experimental setup is shown at dead-bottom position, where the simulated area is identified by a red circle.

The geometry of the finite element model consists of the bottom section of the extrusion process. This is the section which contains the extrusion ledge at the bottom of the die. No further geometry is necessary because the model has been iteratively reduced to capture the significant stresses in the die while tolerating manageable convergence duration. The punch is not modeled; instead, an input displacement is utilized.

The model is partitioned into various sub-sections of the original geometry to focus higher element density to the area of interest which is the internal edges of the mandrel

and die. The mesh is shown in Figure 7. After performing a mesh sensitivity study, the model includes 26,286 elements with 75,785 nodes.

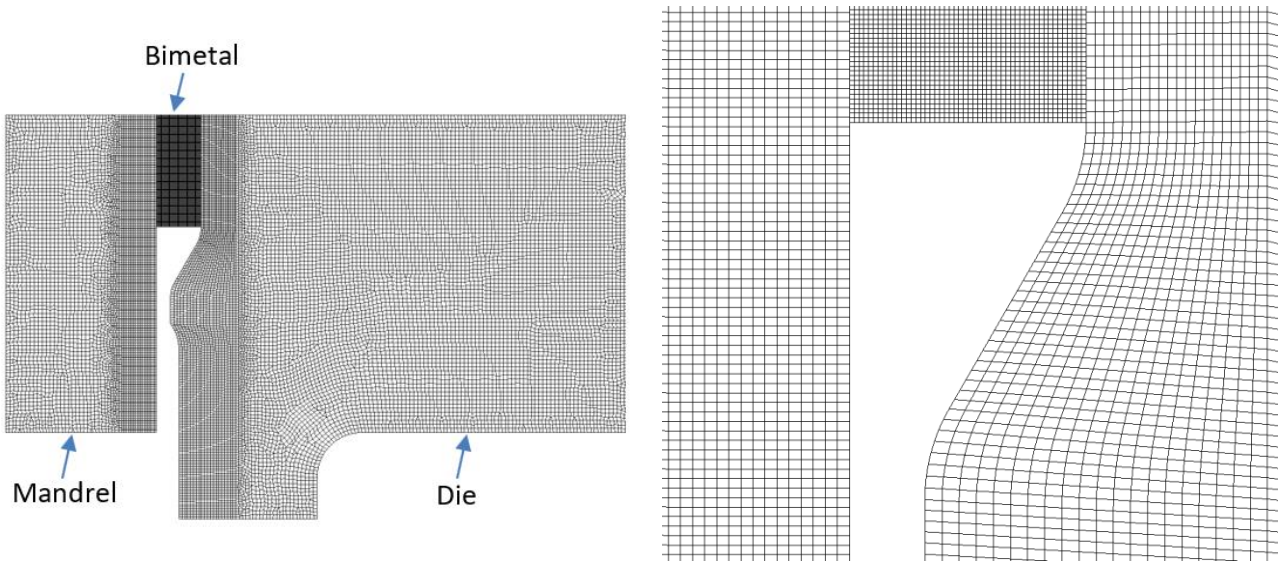

Figure 7. (**a**) The extrusion model meshing, and (**b**) close-up of the meshing, where the metals that will experience extrusion are located at the top of the die ledge at t = 0 s.

The contact control between the die, mandrel, and the metals experiencing extrusion are controlled with an augmented LaGrange formulation with nodal-normal to target detection method. The augmented LaGrange formulation comes with a computational penalty for longer solve time but controls nodal penetration very well, which is important during sliding-type simulation. An allowance of 1.27×10^{-2} mm penetration was tolerated. The contact between the two workpieces is bonded as a simplification to assist in convergence.

A frictional value of 0.025 is used between all sliding surfaces, which is consistent with the conclusions of [65], but slightly less than the values used in other research [66–68]. For comparison to rolling, this frictional value is less than the "normal" lubrication value of 11 as reported in [69]. Unlike rolling, the frictional value must be as low as possible in practice as metal adhesion is a major failure mode in extrusion and is not easily resolved as in rolling. For this reason, the A2 tool steel of the die and mandrel are polished to a 0.8 µm Ra surface finish after a thermally diffused coating of vanadium carbide is applied. The coating has a hardness of 3400 HV minimum and is very smooth. In addition, lubrication is used during testing to reduce the friction coefficient as modeled.

An input displacement of 7.62 mm is applied to the top surfaces of the metals experiencing extrusion which forces them to interact with the extrusion ledge as shown. The input of 7.62 mm is used, as this is sufficient displacement to achieve steady-state plastic flow during the extrusion simulation.

The die and mandrel are evaluated for yielding in four instances where copper-copper and copper-aluminum bimetals are extruded at 52% and 68% deformation. Results are shown in Figure 8. Peak stress occurs on the 30° ledge of the die when extruding copper-copper at 68% deformation where a maximum Von Mises stress is found to be 955 MPa. This demonstrates that a factor-of-safety of 1.7 is achieved in the most stressed condition with the yield strength of 1600 MPa estimated for the die material. Because of this, neither mandrel nor the die are expected to yield. As shown in previous research, a 30° die angle is optimal when compared to 22.5, 45, and 60° angles of similar die design for reducing peak stresses [31].

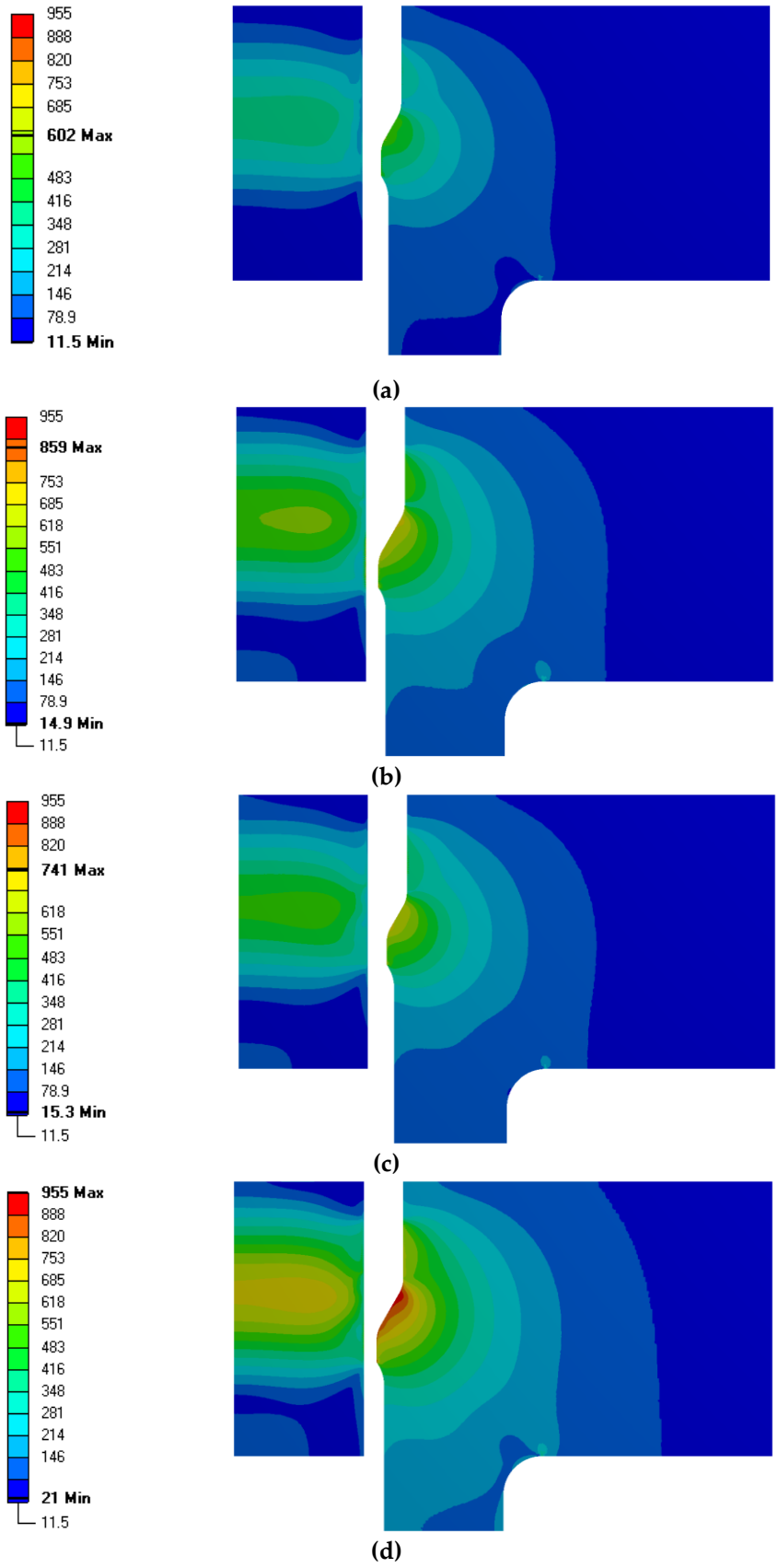

Figure 8. Von Mises stress within the die and mandrel during extrusion of copper-aluminum at (**a**) 52%, and (**b**) 68% deformation and copper-copper at (**c**) 52%, and (**d**) 68% deformation. The metals that experienced extrusion are omitted. Units of stress are MPa.

Steady-state extrusion begins after 4 mm of punch displacement. The peak input force, found at 4.4 mm, is 167 kN as shown in Figure 9 for the copper-copper simulation. Beyond this peak, the input force decreases linearly with a slight negative slope as less bimetal is within the die causing sidewall friction. As shown, the maximum input force is increased by 60.8% for the copper-aluminum bimetal when increasing the deformation from 52% to 68%, and a 55.7% input force increase is observed for the copper-copper bimetal. The predicted peak input force matches the recorded peak input forces within ~1% when averaged across multiple extrusions, where the multiple recorded peak forces are found contained within 5% of the expected peak force.

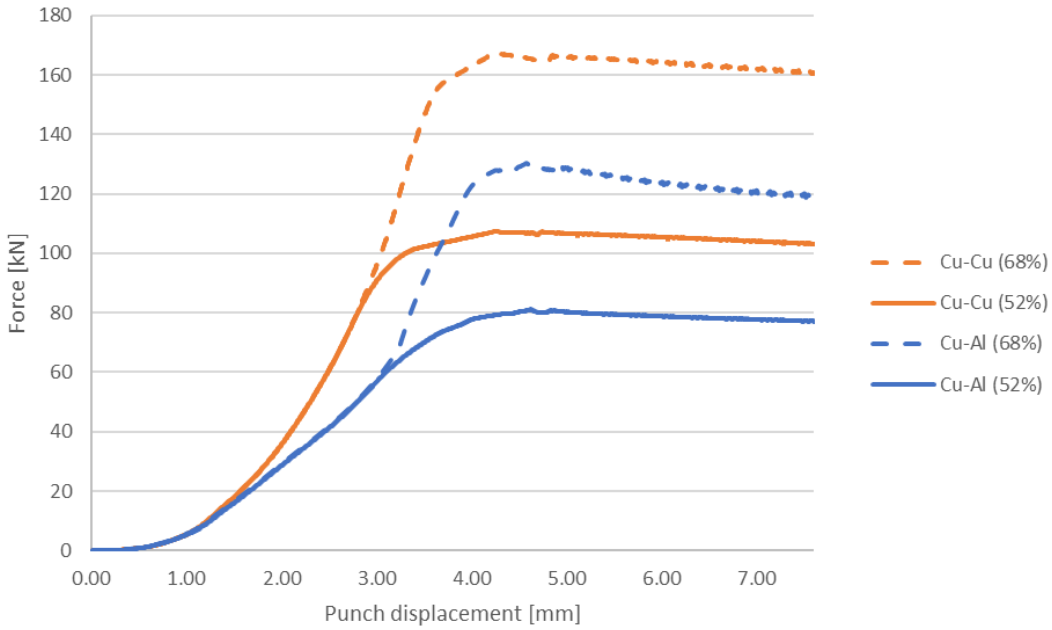

Figure 9. Force-displacement curve for extrusion at 52% and 68% deformation for copper-copper and copper-aluminum bimetals.

As the bimetals pass the extrusion ledge, a significant amount of plastic deformation occurs. The resultant total plastic deformation is shown in Figure 10 for all four cases. In the steady-state extrusion, the plastic strain varies through the thickness and length of the bimetal. Shown in Figure 11 is the plastic strain variance through the wall thickness. In all cases, a higher plastic strain is found on the innermost edge of the tube and decreases close to linearly to the midpoint. Beyond the midpoint, the plastic strain levels out but then dips close to the outer diameter. The innermost metal exhibits higher strain because the outer tube's edge is impacted by the extrusion ledge first, which forces the inner metal to push ahead of the outer metal causing more strain in the inner metal. This is observed in all four cases, and predominately in the 52% deformation case, where the inner material is drawn past the die and is extruded first (reference Figure 10a). Additionally, the layer thickness varies $\pm$ 3% from the nominal thicknesses. Most notable, as observed in Figures 10 and 11, is the drastic increase in plastic strain at the metal-metal interface: 50.1% for copper-copper and 52.6% for copper-aluminum when the deformation is increased from 52% to 68%.

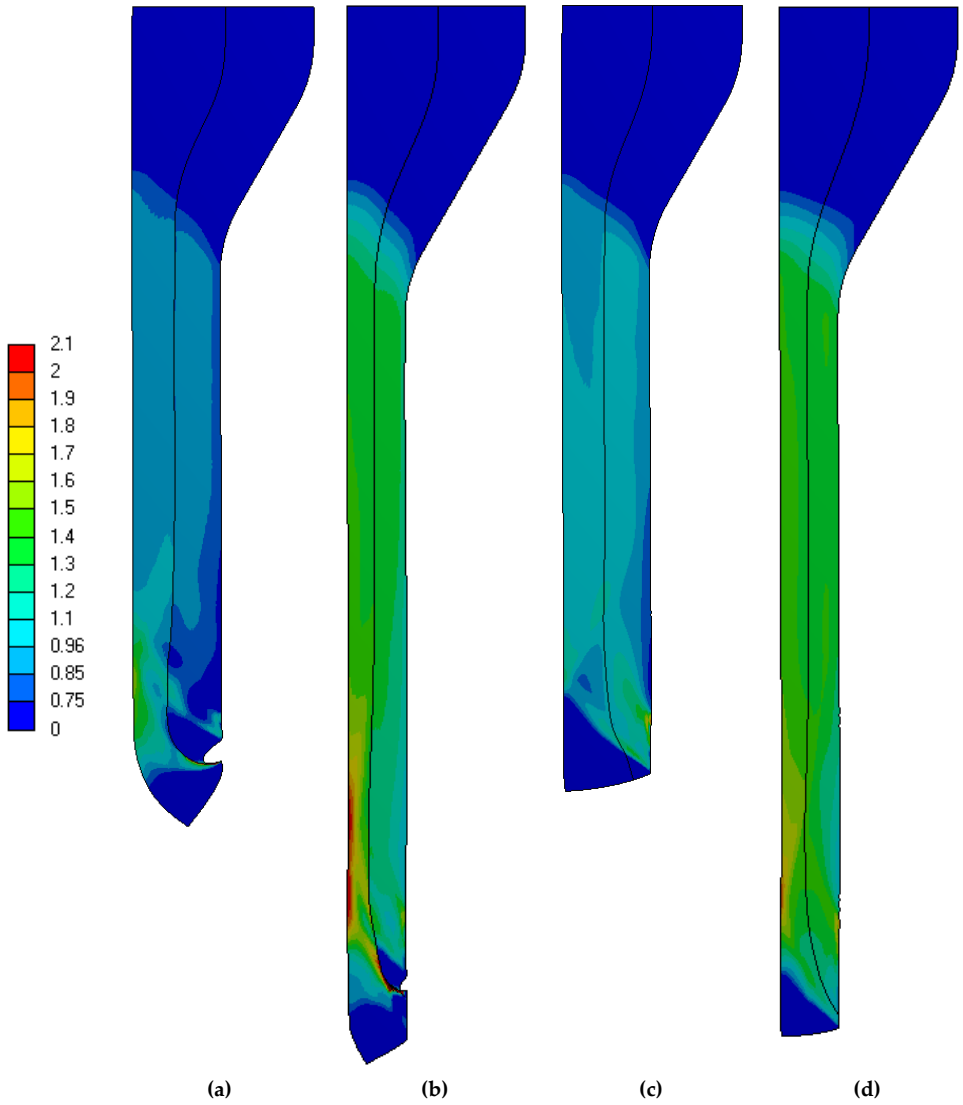

Figure 10. Total equivalent plastic strain at 7.62 mm of displacement for copper-aluminum at (**a**) 52%, and (**b**) 68% deformation and copper-copper at (**c**) 52%, and (**d**) 68% deformation. The die and mandrel are omitted. Units of strain are mm/mm.

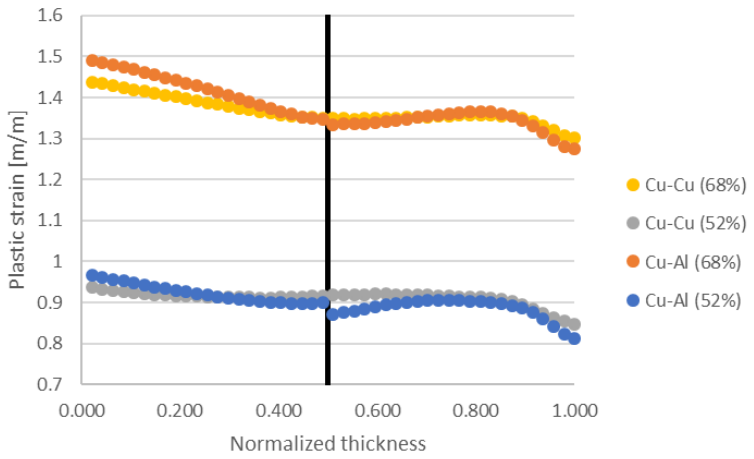

Figure 11. Equivalent plastic strain through the extruded wall where normalized 0.0 is the inner edge of the tubular wall and normalized 1.00 is the outer surface of the tube. Vertical line represents bonding interface location. Plastic strain is taken at the vertical midpoint of the extruded bimetal.

Producing the tubes in this manner requires sacrificing the beginning and end of the extruded tubes. As is evident, the initial section does not fully achieve plastic deformation and the end section is not pressed fully past the extrusion ledge.

6. Results and Discussion

Copper-copper and copper-aluminum bimetallic tubes were produced using the methodology described. The initially stacked copper-copper and copper-aluminum tubes were measured to have an average outer diameter of 28.58 mm and an inner diameter of 22.1 mm before processing. After the AEB process, the outer diameters were reduced to an average of 25.324 mm for the 52% extrusion and 24.257 mm for 68% extrusion. For all extrusions, the inner diameters were found to be 22.073 mm on average. This demonstrates that 49.9% and 66.3% radial deformation was achieved which is less than the targeted 52%, and 68% deformation, respectively. This is due to initial air gaps between the stacked layers, the mandrel, and the die, as well as expansion of the die during extrusion.

Table 7 summarizes all bimetallic tubes produced and whether bonding was achieved or not. The copper-copper tube serves as a baseline and represents the easiest possible chance to achieve full-bonding since metallographic substructures are consistent and the material exhibits identical material behavior. Copper-aluminum, however, represents a combination that is more difficult to bond due to differences in material behavior and different naturally occurring oxide layers. Four-layer tubes of copper-copper, and higher, were not attempted since the 2-layer copper-copper tube demonstrates that bonding is possible using AEB. Further processing of a copper-copper tube would provide no more desired insight as future iterations are expected to bond as the first 2-layer.

Table 7. Summary of bimetallic tubes produced.

	52% Deformation		
Material	**2-layer**	**4-layer**	**8-layer**
copper-aluminum	Yes *	Yes *	Yes *
copper-copper	Yes *		
	68% Deformation		
Material	**2-layer**	**4-layer**	**8-layer**
copper-copper	Yes		

* = no bonding.

Despite adhering to the methodology described above, all samples extruded at 52% did not bond. The only successful bonding occurred at 68% deformation in the copper-copper bimetallic tube. Based on the extrusions performed, deformation greater than 52% is required for bonding since the processing remained constant between all tests. The processing of the 8-layer copper-aluminum tube demonstrates that the extrusion and expansion process can create bimetallic tubes, but deformation percentage needs to be of sufficient strain to enact bonding as shown in the 68% deformed copper-copper tube. Most literature in ARB reports 50% as the low-end of deformation required to enact bonding. Evidently, bonding in the AEB process did not occur at 50% revealing the role of more complex geometry of tube relative to sheet. Mechanical fields in the tube during AEB are different than those in the sheet during ARB making the strain levels required for bonding greater in AEB process than in ARB process.

The copper-aluminum bimetal tube cross-section, shown in extrusion direction, is displayed in Figure 12. As shown in this paper, the layer thickness decreased exponentially, while the tube wall thickness remained constant. Tabulated in Table 8 are the minimum and maximum layer thicknesses measured at the cross-section taken. The 2-layer bimetal tube has very consistent layer thicknesses as well as the 4-layer bimetal. At 8-layers, the layer thickness varied greatly where some layers completely thinned to obsolesce. Beyond this, layer thickness was very inconsistent in the 8-layer bimetal.

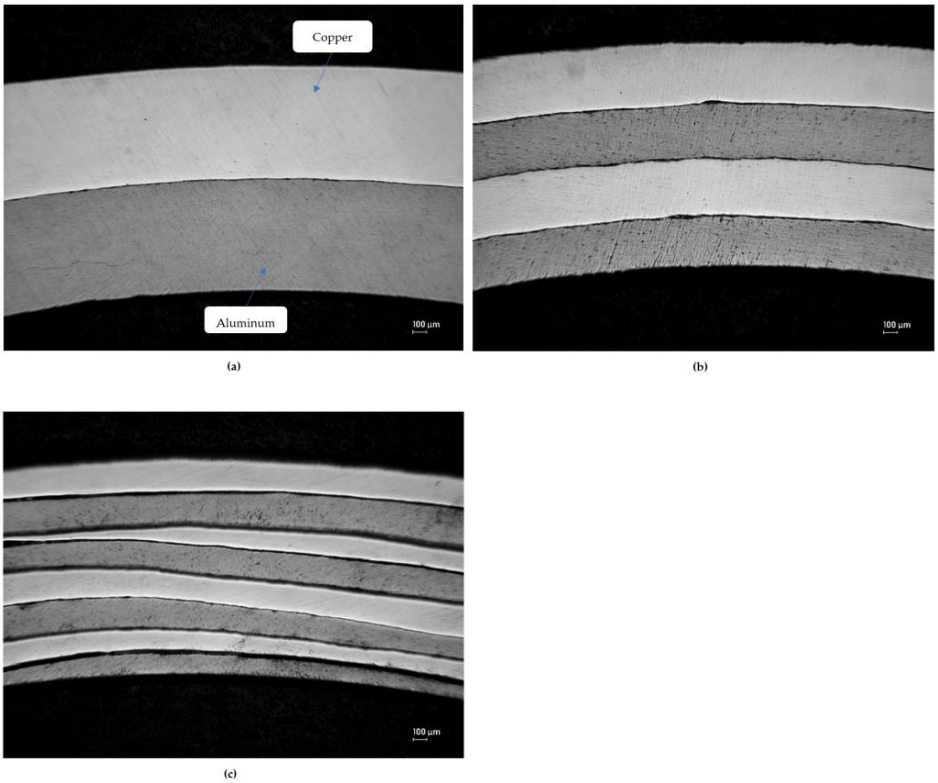

Figure 12. Bimetallic tube of (**a**) 2-layer, (**b**) 4-layer, and (**c**) 8-layer copper-aluminum, shown in the extrusion direction, produced at 52% deformation.

Table 8. Minimum and maximum layer thickness (µm) at 52% deformation.

Layers	**2**		**4**		**8**	
Material	**Cu**	**Al**	**Cu**	**Al**	**Cu**	**Al**
Expected	794	794	396	396	198	198
Average	819	775	414	375	212	200
Minimum	802	743	385	349	0	0
Maximum	847	798	462	402	440	504

In each sample produced at 52% deformation, bonding did not occur and is observed as the dark voids at each interface, as shown in Figure 12. Each subsequent extrusion pass did not further promote bonding as observed in the 8-layer bimetal. For this reason, it is necessary to achieve bonding on the first extrusion iteration. Since bonding did not occur, the material layers acted independently for each future extrusion, and the thin layers did not handle the imposed plastic strain, which ultimately caused significant wrinkling and tearing on the innermost and outermost layers, as well as layer thinning inside the bimetal.

Copper-copper bimetallic tubes were attempted at both 52% and 68% deformation. As mentioned previously, no bonding was achieved at 52% deformation when attempting a copper-copper bimetal. However, using the same method described, bonding was achieved using 68% deformation. As shown in Figure 13, the 2-layer copper-copper bonded interface is observed normal to the extrusion direction. Unlike Figure 12, the copper-copper cross section, shown in Figure 13, required acid-etching to view the interface using microscopy. The layer thickness was measured and found to be 510 µm for the outer layer of copper and 568 µm for the inner layer of copper where the expected thickness was 527 µm. This is attributed to the outer layer being pulled in front of the extrusion ledge during the initial extrusion start which is exhibited predominantly in Figure 10a,b.

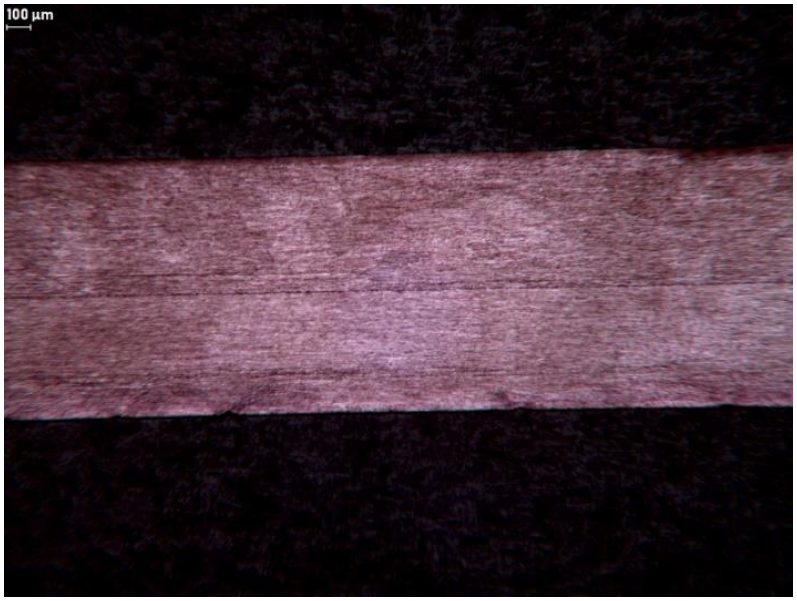

Figure 13. Bimetallic tube of 2-layer copper-copper, shown in the transverse direction, produced at 68% deformation.

Full bonding, however, did not occur as there are voids at the interface. A 15,240 µm long section was surveyed and 85.0% of the length was found to be bonded. In this section, 148 voids were identified with an average length of 15.4 µm. No identifiable pattern was observed regarding the location of the voids, and the largest void was found to be 49.7 µm. Typical voids are shown in Figure 14, which are represented by black at the interface. These voids are expected to collapse during further iterations.

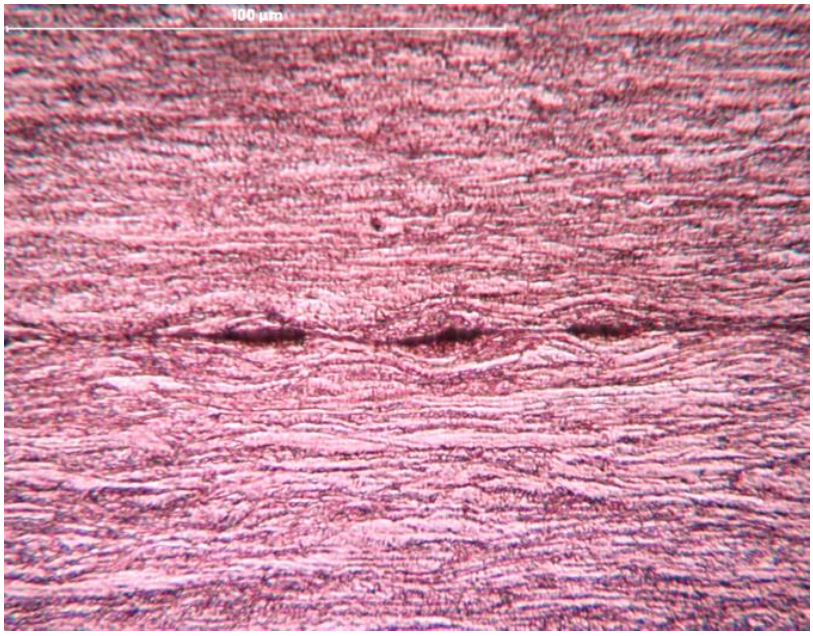

Figure 14. Typical voids found at bonding interface of 2-layer copper-copper tube shown in transverse direction. Bimetal was extruded at 68% deformation.

The grain structure before and after extrusion is displayed in Figure 15. As shown in the transverse direction, the annealed grain structure became highly elongated due to the extrusion process. The copper-copper tube after extrusion is expected to exhibit

an anisotropic material behavior where grains no longer have uniformity in all spatial directions, which is expected for non-heat-treated metal after drawing or extrusion.

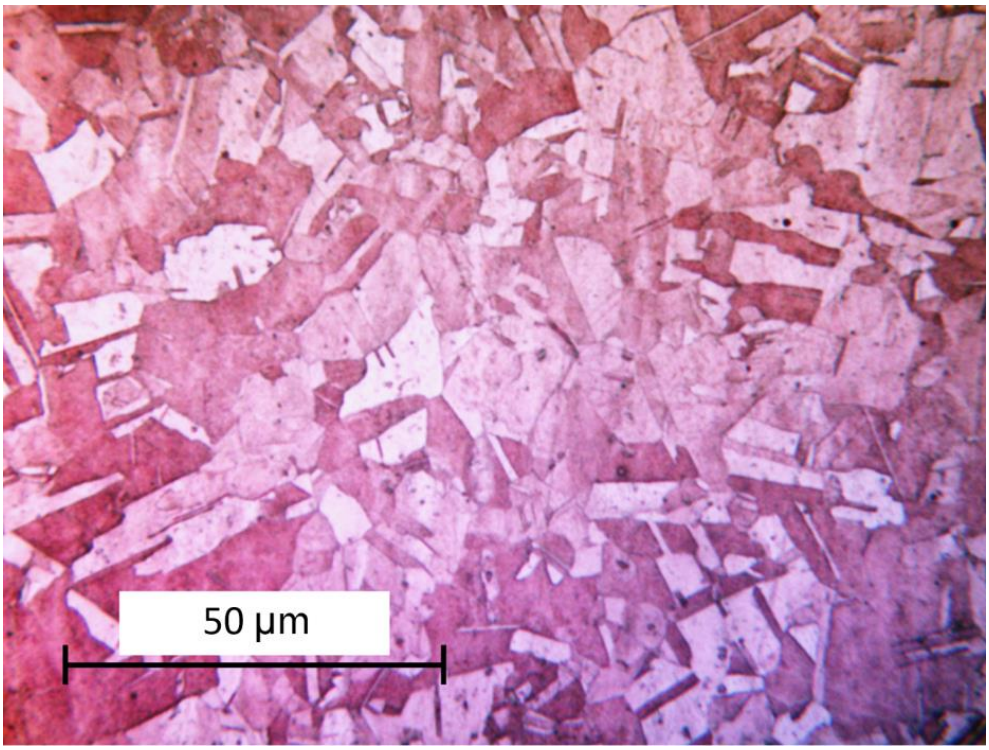

(a)

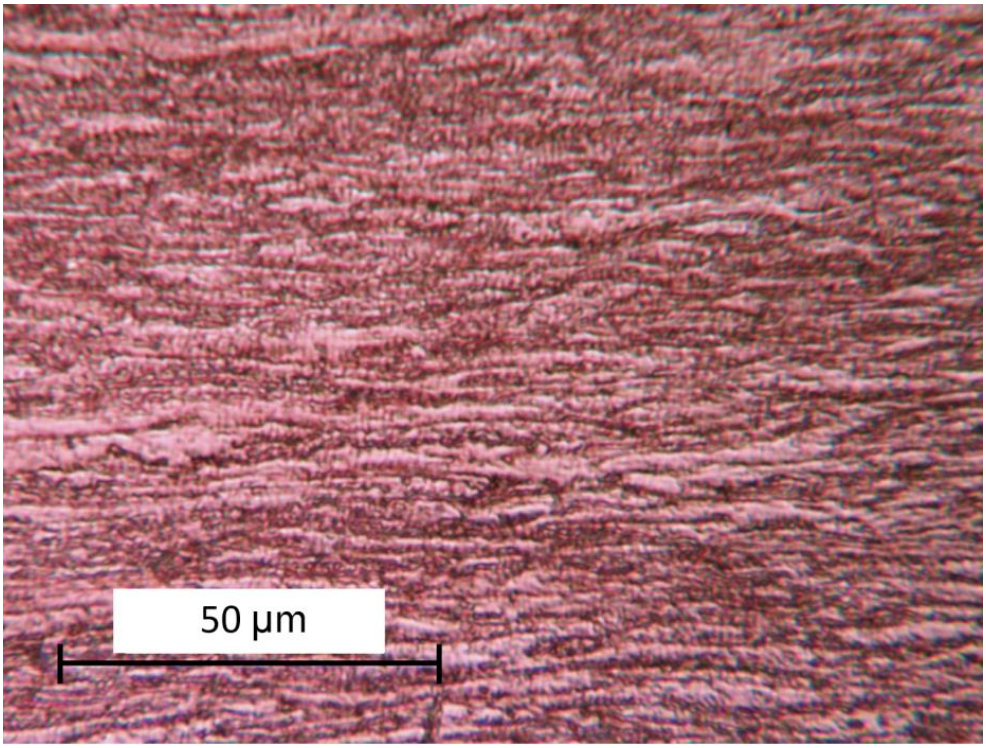

(b)

Figure 15. Microstructure of copper, (**a**) before extrusion, and (**b**) after extrusion at 68% deformation.

The copper-aluminum and copper-copper bimetal underwent significant strain-hardening during extrusion at 52% and 68% deformation. As tabulated in Tables 9 and 10, the hardness of each metal constituent increased significantly. The 8-layer copper-aluminum was not tested for hardness since the individual layers were too small for micro-hardness testing. Interestingly, the copper-copper layers experienced approximately the same increase (165.1% vs. 168.5%) in hardness even though the deformation percentage was 52% and 68% respectively. This suggests there is a hardening limit as no significant increase in hardness was observed with strain.

Table 9. Hardness (HK) before and after extrusion of 2-layer copper-copper bimetal.

Deformation	Annealed	2-Layer	Increase (%)
52%	56.1	148.8	165.1
68%	56.1	150.7	168.5

Table 10. Hardness (HK) before and after extrusion of copper-aluminum bimetal at 52% deformation.

Material	Annealed	2-Layer	Increase (%)	4-Layer	Increase (%)
Copper	56.1	144.0	156.6	146.9	161.9
Aluminum	40.7	72.8	78.9	71.8	76.4

The copper-copper tube, extruded at 68%, exhibits significantly improved material strength as indicated by the material behavior displayed in Figure 16. A second tensile test was performed to confirm results; a difference of ~2% was identified between the two ultimate tensile strengths found. Tensile tests were performed per ASTM E8 using custom sidewall specimens. The 0.2% offset yield strength improved from 83 MPa to 481 MPa; a 480% increase compared to the annealed material. Due to the work hardening experienced during extrusion, ductility is sacrificed for the improved material strength.

The ultimate tensile strength of the copper-copper tube, extruded at 68% using AEB, is compared to pure copper experiencing ARB, as reported by [70], and tube cyclic extrusion-compression (TCEC), as reported by [71]. TCEC is a severe plastic deformation technique where tubes are fully constrained and deformed between an external chamber and an internal mandrel [71]. The pure copper undergoing ARB and TCEC achieved ultrafine grain size after four passes of severe plastic deformation processes. Pure copper experiencing 68% AEB, on the other hand, has a grain size approximately one order of magnitude greater but exhibits the greatest improved ultimate tensile strength in one iteration. The significant improvement of strength is attributed to the hyper-elongated grains shown in Figure 15b, which are oriented in the extrusion direction, where dislocation structures, and underlying residual stress fields expected to form during the process similar to ARB [72]. We observe that grain size obtained is an order of magnitude larger than other severe plastic deformation processes (Table 11), but the largest improvement in ultimate tensile strength was obtained. Therefore, grain size refinement alone does not govern improvements in material strength, but also other features such as dislocation density and low angular boundaries in sub-grain structure also impact strength. Anisotropic material properties are expected since the average grain size is 2.3 μm in the extrusion direction and an average length of 40 μm is in the transverse direction.

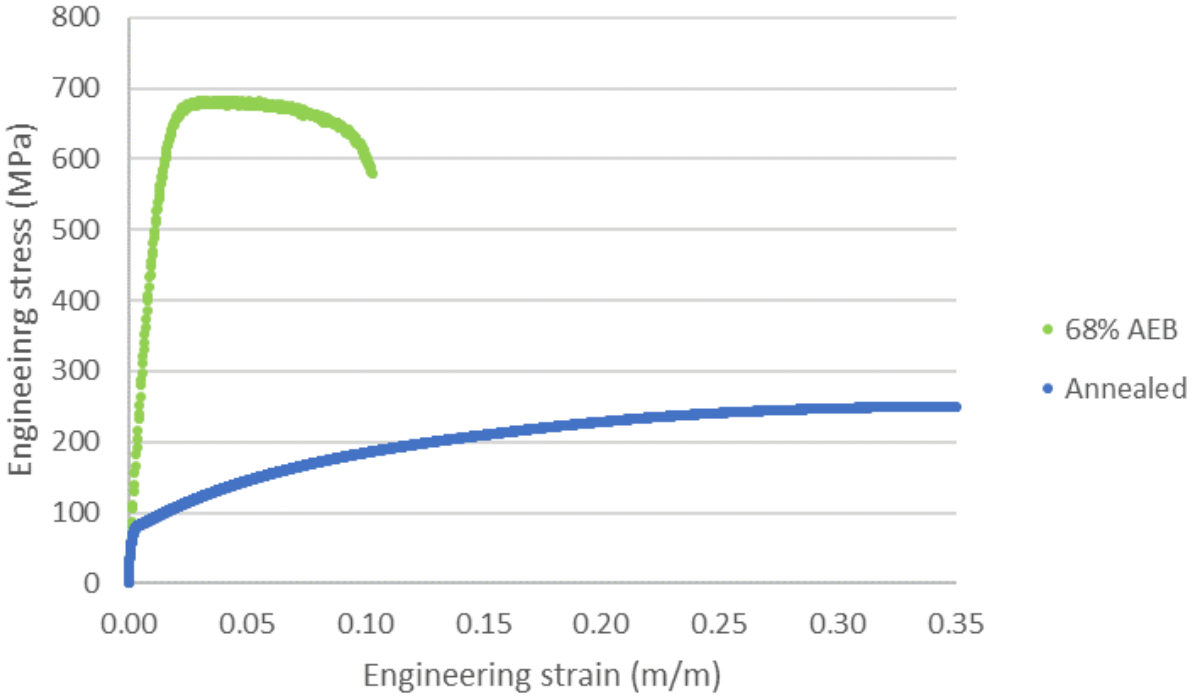

(a)

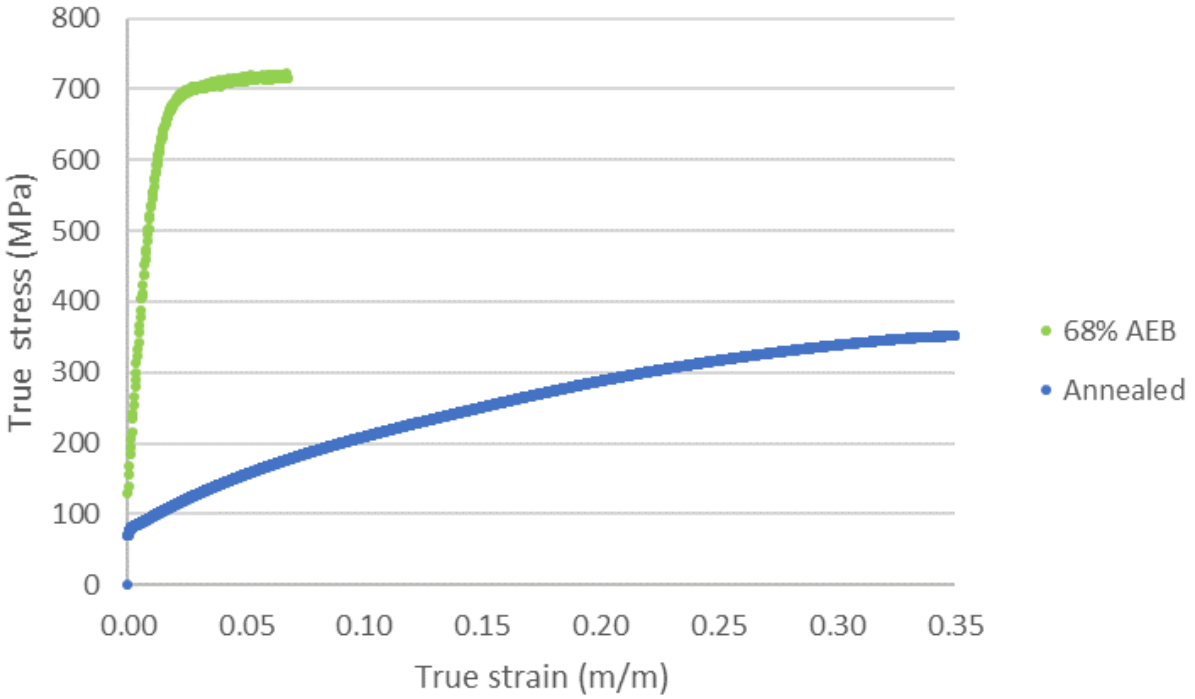

(b)

Figure 16. Engineering stress-strain, (**a**) and true stress-strain, (**b**) of 68% deformation 2-layer copper-copper compared to annealed curves.

Table 11. Ultimate tensile strength of pure copper deformed using different severe plastic deformation processes.

Process	Iteration	Ultimate Tensile Strength (MPa)	Percent Difference to Annealed (%)
68% AEB	1	683	172%
ARB [70]	1	350	39%
ARB [70]	2	370	47%
ARB [70]	3	395	57%
ARB [70]	4	395	57%
TCEC [71]	1	275	10%
TCEC [71]	2	300	20%
TCEC [71]	3	310	24%
TCEC [71]	4	325	29%
Annealed	-	251	0%

7. Summary and Conclusions

This work developed a process termed accumulative extrusion bonding for introducing laminated structures in metallic tubes. To this end, dies are designed and evaluated using the finite element method simulations. Several multilayered tubes are produced using the process and characterized for the extent of bonding, microstructure, hardness, and strength. Significantly, bonding at the interface is achieved for the copper-copper metallic tubing to about 85% at a radial strain of 68% imparted by the AEB process. Since complete bonding is desired, it is recommended to increase the radial deformation to a value greater than 68%. The additional key findings are:

1. Bonding using AEB does not occur at 50% deformation revealing the significant role of more complex geometry of tubes relative to sheets in solid-state bonding. Mechanical fields in the tube during AEB are different from those in the sheet during ARB making the required strain levels for bonding greater in AEB process than those in ARB process.
2. It is necessary to achieve bonding on the first extrusion pass/iteration as future extrusion passes would not promote bonding. Since bonding does not occur on the first extrusion pass at 52% deformation, the material layers act independently for each future extrusion. Moreover, the layers begin to lose their integrity with plastic strain.
3. Surface preparation before forming the interface is very important to facilitate bonding using AEB. Any imperfection left on the interfacial layer will become an inclusion at the interface. During processing it is therefore critical to minimize inadvertent mishandling or extraneous debris. Further processing will thin and stretch areas of contamination but will not remove the inclusions. Moreover, oxidation layer minimization is necessary to aid in bonding. Scratch brushing is used as the process to promote surface hardening while also aiding in the removal of any oxide layer. This method also does not produce any noticeable debris from the bristles which helps promote cleanliness. It is found that over-brushing does not improve the amount of bonding. Beyond scratch brushing, which is a key application to remove oxides and encourage surface hardness, minimizing contact with the atmosphere is also essential.
4. Annealing during each iteration is necessary to remove strain hardening caused during extrusion. Samples extruded with the annealing step omitted failed during extrusion due to wrinkling and tearing.

To achieve unique material properties permitted by ultrafine-laminated structures in tubes like those achieved in sheets, it is necessary to bond different material combinations and further push the layering to the thickness at and below the grain size-level. Future work will explore the possibility to extrusion bond more metal-metal combinations, push the processing to achieve finer layering, and, as necessary, improve the die design.

Author Contributions: Conceptualization, M.R.S. and M.K.; methodology, M.R.S. and M.K.; writing—original draft preparation, M.R.S.; writing—review and editing, M.K. Both authors have read and agreed to the published version of the manuscript.

Funding: This research was funded by the U.S. National Science Foundation (NSF) under Grant No. CMMI-1727495.

Data Availability Statement: The data presented in this study are available on request from the corresponding author. The data cannot be shared at this time due to technical or time limitations.

Acknowledgments: University of New Hampshire for laboratory support and L&S Machine Company LLC for manufacturing die components. The authors also acknowledge support and input from professors Brad L. Kinsey, Jinjin Ha, and Yannis P. Korkolis.

Conflicts of Interest: The authors declare no conflict of interest.

References

1. Bimetallic Tubes. Available online: http://www.beca-engineering.com/product/bimetallictubes.php (accessed on 12 January 2021).
2. Bimetallic Tubes. Available online: https://www.dmitubes.com/bimetallic-tubes.html (accessed on 12 January 2021).
3. New Generation Bimetallic Tubes. Available online: https://www.energetictubes.com/ (accessed on 12 January 2021).
4. Bimetallic Tubes. Available online: https://www.materials.sandvik/en-us/products/tube-pipe-fittings-and-flanges/tubular-products/bimetallic-tubes/ (accessed on 12 January 2021).
5. Hosseini, M.; Pardis, N.; Manesh, H.D.; Abbasi, M.; Kim, D.-I. Structural characteristics of cu/ti bimetal composite produced by accumulative roll-bonding (arb). *Mater. Des.* **2017**, *113*, 128–136. [CrossRef]
6. Jamaati, R.; Toroghinejad, M.R. Manufacturing of high-strength aluminum/alumina composite by accumulative roll bonding. *Mater. Sci. Eng. A* **2010**, *527*, 4146–4151. [CrossRef]
7. Dehsorkhi, R.N.; Qods, F.; Tajally, M. Investigation on microstructure and mechanical properties of al–zn composite during accumulative roll bonding (arb) process. *Mater. Sci. Eng. A* **2011**, *530*, 63–72. [CrossRef]
8. Chang, H.; Zheng, M.; Xu, C.; Fan, G.; Brokmeier, H.; Wu, K. Microstructure and mechanical properties of the mg/al multilayer fabricated by accumulative roll bonding (arb) at ambient temperature. *Mater. Sci. Eng. A* **2012**, *543*, 249–256. [CrossRef]
9. Mahdavian, M.; Ghalandari, L.; Reihanian, M. Accumulative roll bonding of multilayered cu/zn/al: An evaluation of microstructure and mechanical properties. *Mater. Sci. Eng. A* **2013**, *579*, 99–107. [CrossRef]
10. Ghalandari, L.; Mahdavian, M.; Reihanian, M. Microstructure evolution and mechanical properties of cu/zn multilayer processed by accumulative roll bonding (arb). *Mater. Sci. Eng. A* **2014**, *593*, 145–152. [CrossRef]
11. Knezevic, M.; Nizolek, T.; Ardeljan, M.; Beyerlein, I.J.; Mara, N.A.; Pollock, T.M. Texture evolution in two-phase zr/nb lamellar composites during accumulative roll bonding. *Int. J. Plast.* **2014**, *57*, 16–28. [CrossRef]
12. Ardeljan, M.; Beyerlein, I.J.; Knezevic, M. A dislocation density based crystal plasticity finite element model: Application to a two-phase polycrystalline hcp/bcc composites. *J. Mech. Phys. Solids* **2014**, *66*, 16–31. [CrossRef]
13. Savage, D.J.; Beyerlein, I.J.; Mara, N.A.; Vogel, S.C.; McCabe, R.J.; Knezevic, M. Microstructure and texture evolution in mg/nb layered materials made by accumulative roll bonding. *Int. J. Plast.* **2020**, *125*, 1–26. [CrossRef]
14. Leu, B.; Savage, D.J.; Wang, J.; Alam, M.E.; Mara, N.A.; Kumar, M.A.; Carpenter, J.S.; Vogel, S.C.; Knezevic, M.; Decker, R.; et al. Processing of dilute mg–zn–mn–ca alloy/nb multilayers by accumulative roll bonding. *Adv. Eng. Mater.* **2020**, *22*, 1900673. [CrossRef]
15. Mashhadi, A.; Atrian, A.; Ghalandari, L. Mechanical and microstructural investigation of zn/sn multilayered composites fabricated by accumulative roll bonding (arb) process. *J. Alloys Compd.* **2017**, *727*, 1314–1323. [CrossRef]
16. Clemens, B.; Kung, H.; Barnett, S. Structure and strength of multilayers. *MRS Bull.* **1999**, *24*, 20–26. [CrossRef]
17. Mara, N.; Bhattacharyya, D.; Dickerson, P.; Hoagland, R.; Misra, A. Deformability of ultrahigh strength 5 nm cu/nb nanolayered composites. *Appl. Phys. Lett.* **2008**, *92*, 231901. [CrossRef]
18. Zhang, X.; Misra, A.; Wang, H.; Shen, T.; Nastasi, M.; Mitchell, T.; Hirth, J.; Hoagland, R.; Embury, J. Enhanced hardening in cu/330 stainless steel multilayers by nanoscale twinning. *Acta Mater.* **2004**, *52*, 995–1002. [CrossRef]
19. Ardeljan, M.; Knezevic, M.; Jain, M.; Pathak, S.; Kumar, A.; Li, N.; Mara, N.A.; Baldwin, J.K.; Beyerlein, I.J. Room temperature deformation mechanisms of mg/nb nanolayered composites. *J. Mater. Res.* **2018**, *33*, 1311–1332. [CrossRef]
20. Ardeljan, M.; Savage, D.J.; Kumar, A.; Beyerlein, I.J.; Knezevic, M. The plasticity of highly oriented nano-layered zr/nb composites. *Acta. Mater.* **2016**, *115*, 189–203. [CrossRef]
21. Su, Y.; Ardeljan, M.; Knezevic, M.; Jain, M.; Pathak, S.; Beyerlein, I.J. Elastic constants of pure body-centered cubic mg in nanolaminates. *Comput. Mater. Sci.* **2020**, *174*, 109501. [CrossRef]
22. Knezevic, M.; Zecevic, M.; Beyerlein, I.J.; Lebensohn, R.A. A numerical procedure enabling accurate descriptions of strain rate-sensitive flow of polycrystals within crystal visco-plasticity theory. *Comput. Methods Appl. Mech. Eng.* **2016**, *308*, 468–482. [CrossRef]

23. Knezevic, M.; Kalidindi, S.R. Fast computation of first-order elastic-plastic closures for polycrystalline cubic-orthorhombic microstructures. *Comput. Mater. Sci.* **2007**, *39*, 643–648. [CrossRef]
24. Jahedi, M.; Ardjmand, E.; Knezevic, M. Microstructure metrics for quantitative assessment of particle size and dispersion: Application to metal-matrix composites. *Powder Technol.* **2017**, *311*, 226–238. [CrossRef]
25. Misra, A.; Hoagland, R. Effects of elevated temperature annealing on the structure and hardness of copper/niobium nanolayered films. *J. Mater. Res.* **2005**, *20*, 2046–2054. [CrossRef]
26. Bellou, A.; Scudiero, L.; Bahr, D. Thermal stability and strength of mo/pt multilayered films. *J. Mater. Sci.* **2010**, *45*, 354–362. [CrossRef]
27. Han, W.; Misra, A.; Mara, N.; Germann, T.; Baldwin, J.; Shimada, T.; Luo, S. Role of interfaces in shock-induced plasticity in cu/nb nanolaminates. *Philos. Mag.* **2011**, *91*, 4172–4185. [CrossRef]
28. Wei, Q.; Li, N.; Mara, N.; Nastasi, M.; Misra, A. Suppression of irradiation hardening in nanoscale v/ag multilayers. *Acta Mater.* **2011**, *59*, 6331–6340. [CrossRef]
29. Zhernenkov, M.; Jablin, M.S.; Misra, A.; Nastasi, M.; Wang, Y.; Demkowicz, M.J.; Baldwin, J.K.; Majewski, J. Trapping of implanted he at cu/nb interfaces measured by neutron reflectometry. *Appl. Phys. Lett.* **2011**, *98*, 241913. [CrossRef]
30. Lesuer, D.; Syn, C.; Sherby, O.; Wadsworth, J.; Lewandowski, J.; Hunt, W. Mechanical behaviour of laminated metal composites. *Int. Mater. Rev.* **1996**, *41*, 169–197. [CrossRef]
31. Knezevic, M.; Jahedi, M.; Korkolis, Y.P.; Beyerlein, I.J. Material-based design of the extrusion of bimetallic tubes. *Comput. Mater. Sci.* **2014**, *95*, 63–73. [CrossRef]
32. Valiev, R.Z.; Estrin, Y.; Horita, Z.; Langdon, T.G.; Zechetbauer, M.J.; Zhu, Y.T. Producing bulk ultrafine-grained materials by severe plastic deformation. *JOM* **2006**, *58*, 33–39. [CrossRef]
33. Knezevic, M.; Bhattacharyya, A. Characterization of microstructure in nb rods processed by rolling: Effect of grooved rolling die geometry on texture uniformity. *Int. J. Refract. Met. Hard Mater.* **2017**, *66*, 44–51. [CrossRef]
34. Kalidindi, S.R.; Duvvuru, H.K.; Knezevic, M. Spectral calibration of crystal plasticity models. *Acta Mater.* **2006**, *54*, 1795–1804. [CrossRef]
35. Jahedi, M.; Knezevic, M.; Paydar, M. High-pressure double torsion as a severe plastic deformation process: Experimental procedure and finite element modeling. *J. Mater. Eng. Perform.* **2015**, *24*, 1471–1482. [CrossRef]
36. Jahedi, M.; Beyerlein, I.J.; Paydar, M.H.; Knezevic, M. Effect of grain shape on texture formation during severe plastic deformation of pure copper. *Adv. Eng. Mater.* **2018**, *20*, 1600829.
37. Jahedi, M.; Beyerlein, I.J.; Paydar, M.H.; Zheng, S.; Xiong, T.; Knezevic, M. Effects of pressure and number of turns on microstructural homogeneity developed in high-pressure double torsion. *Metall. Mater. Trans. A* **2017**, *48*, 1249–1263. [CrossRef]
38. Jahedi, M.; Paydar, M.H.; Knezevic, M. Enhanced microstructural homogeneity in metal-matrix composites developed under high-pressure-double-torsion. *Mater. Charact.* **2015**, *104*, 92–100. [CrossRef]
39. Jahedi, M.; Paydar, M.H.; Zheng, S.; Beyerlein, I.J.; Knezevic, M. Texture evolution and enhanced grain refinement under high-pressure-double-torsion. *Mater. Sci. Eng. A* **2014**, *611*, 29–36. [CrossRef]
40. Qiao, X.G.; Gao, N.; Starink, M.J. A model of grain refinement and strengthening of al alloys due to cold severe plastic deformation. *Philos. Mag.* **2012**, *92*, 446–470. [CrossRef]
41. Bachmaier, A.; Pippan, R. Generation of metallic nanocomposites by severe plastic deformation. *Int. Mater. Rev.* **2013**, *58*, 41–62. [CrossRef]
42. Xu, C.; Xia, K.; Langdon, T.G. The role of back pressure in the processing of pure aluminum by equal-channel angular pressing. *Acta Mater.* **2007**, *55*, 2351–2360. [CrossRef]
43. Harsha, R.; Kulkarni, V.M.; Babu, B.S. Severe plastic deformation-a review. *Mater. Today Proc.* **2018**, *5*, 22340–22349. [CrossRef]
44. Valiev, R.; Korznikov, A.; Mulyukov, R. Structure and properties of ultrafine-grained materials produced by severe plastic deformation. *Mater. Sci. Eng. A* **1993**, *168*, 141–148. [CrossRef]
45. Sadasivan, N.; Balasubramanian, M. Severe plastic deformation of tubular materials–process methodology and its influence on mechanical properties–a review. *Mater. Today Proc.* **2021**. [CrossRef]
46. Zare, H.; Jahedi, M.; Toroghinejad, M.R.; Meratian, M.; Knezevic, M. Microstructure and mechanical properties of carbon nanotubes reinforced aluminum matrix composites synthesized via equal-channel angular pressing. *Mater. Sci. Eng. A* **2016**, *670*, 205–216. [CrossRef]
47. Zare, H.; Jahedi, M.; Toroghinejad, M.R.; Meratian, M.; Knezevic, M. Compressive, shear, and fracture behavior of cnt reinforced al matrix composites manufactured by severe plastic deformation. *Mater. Des.* **2016**, *106*, 112–119. [CrossRef]
48. Chen, X.; Huang, G.; Liu, S.; Han, T.; Jiang, B.; Tang, A.; PAN, F.; ZHU, Y. Grain refinement and mechanical properties of pure aluminum processed by accumulative extrusion bonding. *Trans. Nonferrous Met. Soc. China* **2019**, *29*, 437–447. [CrossRef]
49. Chen, X.; Xia, D.; Zhang, J.; Huang, G.; Liu, K.; Tang, A.; Jiang, B.; Pan, F. Ultrafine-grained al–zn–mg–cu alloy processed via cross accumulative extrusion bonding and subsequent aging: Microstructure and mechanical properties. *J. Alloys Compd.* **2020**, *846*, 156306. [CrossRef]
50. Chen, X.; Zhang, J.; Xia, D.; Huang, G.; Liu, K.; Jiang, B.; Tang, A.; Pan, F. Microstructure and mechanical properties of 1060/7050 laminated composite produced via cross accumulative extrusion bonding and subsequent aging. *J. Alloys Compd.* **2020**, *826*, 154094. [CrossRef]

51. Liu, S.; Zhang, J.; Chen, X.; Huang, G.; Xia, D.; Tang, A.; Zhu, Y.; Jiang, B.; Pan, F. Improving mechanical properties of heterogeneous mg-gd alloy laminate via accumulated extrusion bonding. *Mater. Sci. Eng. A* **2020**, *785*, 139324. [CrossRef]
52. Mehr, V.Y.; Toroghinejad, M.R.; Rezaeian, A. The effects of oxide film and annealing treatment on the bond strength of al–cu strips in cold roll bonding process. *Mater. Des.* **2014**, *53*, 174–181. [CrossRef]
53. Ana, S.A.; Reihanian, M.; Lotfi, B. Accumulative roll bonding (arb) of the composite coated strips to fabricate multi-component al-based metal matrix composites. *Mater. Sci. Eng. A* **2015**, *647*, 303–312. [CrossRef]
54. Mozaffari, A.; Hosseini, M.; Manesh, H.D. Al/ni metal intermetallic composite produced by accumulative roll bonding and reaction annealing. *J. Alloys Compd.* **2011**, *509*, 9938–9945. [CrossRef]
55. Jamaati, R.; Toroghinejad, M.R. Effect of friction, annealing conditions and hardness on the bond strength of al/al strips produced by cold roll bonding process. *Mater. Des.* **2010**, *31*, 4508–4513. [CrossRef]
56. Chitkara, N.; Aleem, A. Extrusion of axi-symmetric bi-metallic tubes from solid circular billets: Application of a generalised upper bound analysis and some experiments. *Int. J. Mech. Sci.* **2001**, *43*, 2833–2856. [CrossRef]
57. Chaudhari, G.; Andhale, S.; Patil, N. Experimental evaluation of effect of die angle on hardness and surface finish of cold forward extrusion of aluminum. *Int. J. Emerg. Technol. Adv. Eng.* **2012**, *2*, 334–338.
58. Vaidyanath, L.; Nicholas, M.; Milner, D. Pressure welding by rolling. *Br. Weld. J.* **1959**, *6*, 13–28.
59. Hua, F.; Yang, Y.; Zhang, Y.; Guo, M.; Guo, D.; Tong, W.; Hu, Z. Three-dimensional finite element analysis of tube spinning. *J. Mater. Process. Technol.* **2005**, *168*, 68–74. [CrossRef]
60. Xia, Q.; Xie, S.W.; Huo, Y.; Ruan, F. Numerical simulation and experimental research on the multi-pass neck-spinning of non-axisymmetric offset tube. *J. Mater. Process. Technol.* **2008**, *206*, 500–508. [CrossRef]
61. Ardeljan, M.; Knezevic, M.; Nizolek, T.; Beyerlein, I.J.; Mara, N.A.; Pollock, T.M. A study of microstructure-driven strain localizations in two-phase polycrystalline hcp/bcc composites using a multi-scale model. *Int. J. Plast.* **2015**, *74*, 35–57. [CrossRef]
62. Dallas, D.B. *Tool and Manufacturing Engineers Handbook*, 3rd ed.; McGraw Hill Inc.: New York, NY, USA, 1976.
63. McCauley, E.O.A.C.J. *Tool Steels*, 28th ed.; Industrial Press Inc.: New York, NY, USA, 2008.
64. Thermal Diffusion (VCTDH) Coatings. Available online: https://www.ibccoatings.com/thermal-diffusion-td-coatings (accessed on 12 January 2021).
65. de Moraes Costa, A.L.; da Silva, U.S.; Valberg, H.S. On the friction conditions in fem simulations of cold extrusion. *Procedia Manuf.* **2020**, *47*, 231–236. [CrossRef]
66. Zecevic, M.; McCabe, R.J.; Knezevic, M. A new implementation of the spectral crystal plasticity framework in implicit finite elements. *Mech. Mater.* **2015**, *84*, 114–126. [CrossRef]
67. Knezevic, M.; Beyerlein, I.J. Multiscale modeling of microstructure-property relationships of polycrystalline metals during thermo-mechanical deformation. *Adv. Eng. Mater.* **2018**, *20*, 1700956. [CrossRef]
68. Knezevic, M.; Kalidindi, S.R. Crystal plasticity modeling of microstructure evolution and mechanical fields during processing of metals using spectral databases. *JOM* **2017**, *69*, 830–838. [CrossRef]
69. Madaah-Hosseini, H.; Kokabi, A. Cold roll bonding of 5754-aluminum strips. *Mater. Sci. Eng. A* **2002**, *335*, 186–190. [CrossRef]
70. Fattah-Alhosseini, A.; Imantalab, O.; Mazaheri, Y.; Keshavarz, M. Microstructural evolution, mechanical properties, and strain hardening behavior of ultrafine grained commercial pure copper during the accumulative roll bonding process. *Mater. Sci. Eng. A* **2016**, *650*, 8–14. [CrossRef]
71. Babaei, A.; Mashhadi, M. Tubular pure copper grain refining by tube cyclic extrusion–compression (tcec) as a severe plastic deformation technique. *Prog. Nat. Sci. Mater. Int.* **2014**, *24*, 623–630. [CrossRef]
72. Alvandi, H.; Farmanesh, K. Microstructural and mechanical properties of nano/ultra-fine structured 7075 aluminum alloy by accumulative roll-bonding process. *Procedia Mater. Sci.* **2015**, *11*, 17–23. [CrossRef]